The role of Au, Cu & CeO_2 and their interactions for an enhanced WGS performance

T.R. Reina[1*], S. Ivanova, M.A. Centeno and J.A. Odriozola

Departamento de Química Inorgánica, Universidad de Sevilla e Instituto de Ciencias de Materiales de Sevilla Centro mixto US-CSIC Avda. Américo Vespucio 49, 41092 Seville, Spain.

(*) corresponding author: t.ramirez-reina@imperial.ac.uk

Abstract

The WGS reaction over multicomponent $Au/Ce_{1-x}Cu_xO_2/Al_2O_3$ catalysts is studied in this work. The systems are carefully designed aiming to take advantage of every active phase included in the formulation: gold, ceria and copper. Special emphasis is given to the CeO_2-CuO synergy and its influence on the displayed catalytic performance with and without gold. To this aim a meaningful correlation between the physicochemical properties of the mixed materials and their activity/stability is proposed. In general terms the developed catalysts present high activity under realistic WGS reaction conditions, with fairly good long term stability. In addition, the systems successfully withstand start-up/shut-downs situations, indispensable requisite for real applications in the field of pure hydrogen production for fuel cell goals.

Keywords: WGS, gold catalysts, cerium oxide, copper oxide.

[1]Actual corresponding author address: Department of Chemical Engineering, Imperial College London, London SW7 2AZ.

1. Introduction

Bulk metallic gold is commonly known due to its high inertness and non-changing character being ideal for jewelry proposes. Its low chemical and catalytic activity converts gold in the least reactive transition metal, so that it is often referred to as the "coinage metal" [1-3]. However, gold becomes extremely active when subdivided into nanoscale (usually less than 5 nm) and dispersed over an adequate metal oxide and/or activated carbon supports [4-8]. Nanogold based catalysts have demonstrated outstanding efficiency in a broad range of catalytic reactions including hydrogenation, complete and selective oxidation and nucleophilic addition among other processes [7].

In particular, a stretch relationship between gold and the WGS reaction started twenty years ago with the seminal work of Andreev's group in which they report a very good performance of Au/ Fe_2O_3 catalysts [9]. From then on, WGS and gold based catalysts have evolved together with a marked influence of the emerging hydrogen technologies and the use of the shift reaction as a fundamental stage gate for the pure hydrogen production [10]. In this context, the nature of the support and the effects of metal ↔ support interactions (i.e. charge transfer between the oxide and gold) are of paramount importance to produce well performing gold based catalysts for the WGS reaction [3]. Despite the broad range of supports traditionally employed for gold nanoparticles, there is a general agreement that redox active supports are the most suitable ones. In particular, ceria has attracted big attention due to its excellent behavior in oxidation reactions and it is one of the most appropriate supports for the WGS [11-14].

The combination of ceria with Cu/CuO species has been also proposed as promising catalyst for the WGS and the preferential CO oxidation (PrOx) in both direct (Cu/CeO_2) and inverse

configuration (CeO_2/Cu) [15,16]. The excellent activity of both type of configuration underlines the importance of the metal/oxide interface as a "hot spot" where most of the relevant reaction steps take place. As indicated by Flytzani-Stephanopoulos et al. [17] a redox reaction mechanism can be imagined for these Cu/CeO_2 systems. This process involves the oxidation of CO adsorbed on the Cu cluster by oxygen supplied to the metal interface by ceria, followed by H_2O filling of the oxygen vacancies on ceria. It is therefore desirable a fast oxygen migration from ceria to Cu sites at the metal-support interface. Furthermore, Cu itself is rather active for the shift reaction and indeed it is regarded as the active phase in the state of the art WGS catalyst in the low temperature regime (Cu/ZnO/Al_2O_3) [10].

On the other hand, the nano size of the ceria and copper particles is a key factor governing the catalytic activity [15]. In this regard, highly dispersed ceria particles with small particle size can be achieved by supporting ceria on a high surface carrier as carbon or alumina [18, 19]. This approach also leads to enhanced oxygen mobility and reduces ceria expense while increasing the metal-surface extension due to the smaller size of the oxide crystal. The same behaviour is expected for CeO_2-CuO mixed systems, converting CeO_2-CuO/Al_2O_3 combinations into ideal supports and/or co-catalysts for gold nanoparticles.

In this scenario, a new family of carefully designed Au/$Ce_{1-x}Cu_xO_2$/Al_2O_3 catalysts for the WGS reaction is proposed in this work. The systems are studied under realistic conditions and submitted to demanding stability tests targeting a hypothetical application in the field of fuel cells. The effect of the Au-support interaction and the physicochemical phenomena behind the Ce-Cu synergy are also a subject of this study due to their strong impact on the catalytic performance.

2. Experimental

2.1. Catalyst preparation

Support preparation

The supports were synthesized by co-impregnation method. The necessary amounts of metal nitrate precursor (cerium and copper nitrates, Sigma-Aldrich) were co-impregnated on γ-alumina powder (Sasol). The impregnation was carried out in 50 mL of ethanol, evaporated at reduced pressure in rotary evaporator (Heidolph) at 50 ºC till obtaining a dry solid. The support was then filtered, dried and calcined at 500 ºC during 4 hours. The intended composition of the samples was 15 wt. % of Ce-Cu mixed oxide dispersed on alumina with a diverse $Ce_xCu_{1-x}O_2$ stoichiometry. For sake of simplicity subscripts and decimals have been replaced by entire numbers and oxygen is omitted in the selected nomenclature. For example, the support labelled as Ce8Cu2/Al contains 15 % of Ce-Cu mixed oxide with the stoichiometry $Ce_{0.8}Cu_{0.2}O_2$ dispersed on Al_2O_3.

Gold deposition

Gold was deposited by the direct anionic exchange method (DAE), assisted by NH_3 as described in literature [20]. A 10^{-4} mol L^{-1} aqueous solution of the gold precursor $HAuCl_4$ (Alfa Aesar) was used in order to obtain a final Au loading of 2 wt. %. The support was sieved and the 100-200 μm fractions retained was used to prepare the gold based catalysts. After Au deposition, the solid was dried at 100 °C overnight and calcined in air at 350°C for 4 h.

2.2. Catalyst characterization

X-ray microfluorescence spectrometry (XRMF) was used to determine the chemical compositions and the analysis was performed in EDAX Eagle III spectrophotometer with Rh source of radiation.

The specific surface area was determined by N_2 adsorption-desorption measurements at liquid nitrogen temperature. The experiments were carried out on a Micrometrics Tristar II instrument. Before the analysis, the samples were degassed for 2h at 250 ºC in vacuum. BET equation was applied to obtain the specific surface area of the studied samples.

X-ray diffraction (XRD) analysis was carried out on X`Pert Pro PANalytical instrument. Diffraction patterns were recorded using Cu Kα radiation (40 mA, 45kV) over a 2θ-range of 10 to 80º and using a step size of 0.05º and a step time of 240 s.

The Raman spectra were recorded in a dispersive Horiva Jobin Yvon LabRam HR800 spectrometer, with a 20 mW He–Ne green laser (532.14 nm) operating at 5 mW. The microscope used a 50x objective and a confocal pinhole of 1000 µm.

The UV-Vis spectra were recorded on an Avantes spectrometer model AvaLight-DH-S-BAL and using $BaSO_4$ as reference. All the spectra were collected in a diffuse reflectance mode and transformed to a magnitude proportional to the extinction coefficient through the Kubelka-Munk function F(α). From UV-data, ceria band gap was estimated by plotting $[(F(R)h\nu]^{1/2}$ against energy and the linear part of the curve further extrapolated to $[(F(R)h\nu]^{1/2} = 0$

For the oxygen storage capacity (OSC) measurements 100 mg of catalyst were loaded and activated into a U-shaped quartz reactor at 350 ºC during 1 hour in 5% O_2/ He flow (50 mL/min). Then, the system is cooled and set to the desired temperature (200, 250 and 300 ºC). For each temperature, ten O_2 pulses of 1 mL were injected every 2 min. The sample is then subjected after 10 min He degasification to four alternating series of pulses ($CO–O_2–CO–O_2–CO–O_2$-$CO–O_2$). The OSC is determined by the average amount of CO_2 per pulse formed after the first CO pulse of the alternated ones. This methodology is adapted from previous works published by Duprez *et al.* [21,22]. The gas composition at the exit of the reactor was analyzed by a mass spectrometer PFEIFFER Vacuum PrismaPlus controlled by Quadera® software.

Several assumptions were contemplated for the OSC calculations. Concretely, it was considered that i) only oxygen atoms bonded to the cerium participate in the oxygen storage process; ii) the surface is assumed homogeneous iii) only one of the four oxygen atoms of ceria is involved in the storage ($CeO_2 \rightarrow Ce_2O_3$ + "O"); same for copper oxide ($CuO \rightarrow Cu$ + "O") and iv) null gold metal contribution to the reduction, e.g. the gold metal could not be reoxidized. Similar assuptions to estimate the overall OSC were reported elesewhere [19]. Furthermore, a possible underestimation of OSC due to carbonates formation would be rather equal for all samples allowing a meaningul comparision.

Temperature-programmed desorption (TPD) experiments were performed in a homemade apparatus coupled to a mass spectrometer Thermostar-QMS 200, Pfeiffer Vacuum. The m/e ratios in the 2-60 range were registered but only m/e = 44 (CO_2) signal is represented. 80 mg of the samples were heated in 25 mL/min flowing argon up to 800 °C at 10 ° C/min.

2.3. Catalytic Activity

Water-gas shift reaction was performed in a stainless steel tubular flow reactor (0.75 cm ID) at atmospheric pressure in the 140-350 ºC temperature range. The catalysts were pelletized and sieved with the 600-800 μm fraction employed for the test. The following conditions were applied: catalyst bed volume 1.5 cm^3, space velocity 4000 h^{-1} and gas composition: 30% vol. H_2O + 4.5% vol. CO balance in N_2. Water was injected into flowing gas stream by HPLC pump, vaporized and homogenized with the gas feed before entering the reactor. The CO and CO_2 content was determined by on line ABB gas analyzer and the activity expressed in terms of CO conversion. Diffusion limitation tests were investigated over a gold-based catalyst similar to the ones presented in this study and using different particle sizes (100-200 μm, 420-500 μm, and 600-800 μm). The catalytic activity was rather similar in the whole temperature range for all the tested particle sizes pointing the absence of internal mass transport resistances in our set-up.

The most active samples were studied using gas composition imitating the outlet of an ethanol reformer: 30% H_2O, 9% CO, 11% CO_2 and 50% H_2. The start-up/shutdown tests were carried out by cooling the system until room temperature without interrupting the WGS flow. Once the system reaches room temperature the reaction feed was passed through the catalytic bed during 30 min. Afterwards, the reactor was heated to the chosen temperature (280 ºC)

Results and discussion

Specific surface area and chemical analysis

The specific surface area and the chemical composition of the prepared gold based catalysts are presented in Table 1. The samples are mesoporous materials with textural properties basically given by the primary alumina support (220 m^2/g). The Au/Al catalyst presented the highest S_{BET}. When CeO_2, CuO or a Ce-Cu mixed oxide are added, the specific surface area sensibly drops. However all the ceria and/or copper containing samples presented a comparable S_{BET} value.

As for the chemical composition, the elemental analysis reveals that the samples are mainly composed by alumina (*ca.* 85 wt. % for all the catalysts) with copper oxide and ceria loading close to 15 wt. % as intended in the synthesis and with the Ce/Cu ratio varying according to the targeted stoichiometry. Regarding gold loadings, some interesting differences were found. Firstly, the Au/Al system seems to be the catalyst with the poorest capacity to incorporate gold. Actually this behavior was previously observed elsewhere [23] and it seems to be related with the mechanism of gold incorporation when the direct anionic exchange method assisted by NH_3 is applied. Apparently, the presence of CeO_2 benefits gold uptake as can be intended from the gold loadings found for the Ce-Cu mixed systems. Gold concentration decreases upon increasing the copper proportion in the mixed oxide. The greater gold uptake could be related to the ceria oxygen vacancies. It has been broadly reported that these oxygen punctual defects are electron rich sites where gold nanoparticles preferentially nucleate. In this sense, higher concentration of oxygen vacancies may result in an optimum gold uptake and a strong Au-CeO_2 contact [19, 24].

X-Ray diffraction (XRD)

Crystalline phase composition of the prepared materials was analyzed with XRD. Figure 1A shows the XRD diffraction patterns of the prepared supports. All the samples present the typical reflexions of the main support γ-Al_2O_3 phase (JCPDS# 00-048-0367). Ceria containing samples show the characteristic peaks of the fluorite cubic structure (JCPDS# 00-004-0593) while some peaks related to monoclinic CuO (JCPDS# 80-1917) were detected in some of the samples. The presence of copper started to be noticeable in the XRD for high copper loadings Ce2Cu8/Al and Cu/Al support. For the Ce5Cu5/Al and for the Ce8Cu2/Al no signals of copper were detected indicating a small particle size and well dispersion of copper particles or the possible incorporation of Cu cations in the ceria lattice. Indeed some variations in the ceria cell parameter of the catalysts were detected as indicated in Table 1. This observation suggests a certain degree of copper incorporation on the ceria lattice. The observed contraction of the fluorite cell is then related to the smaller size of Cu^{2+} cations in comparison with Ce^{4+} (77 vs 101 pm). This result agrees with previous synchrotron derived XRD data for $Ce_{1-x}Cu_xO_2$ catalysts where the substitutional Cu^{2+} incorporation into the ceria lattice along with the formation of oxygen vacancies for balance charge mechanism was claimed [25]

The addition of gold did not drive to any detectable modification in the XRD diffraction patterns. No signals attributed to crystalline gold species were detected, as an indication of good dispersion and small nanogold paricle size achieved with this preparation method in good concordance with previous studies [19, 20, 26]. It should be also commented that ceria particle size decreases with copper loading up to a limit that is reached for the Au/Ce2Cu8/Al composition (Table 1). This result indicates a higher dispersion and greater Au-CeO_2 and CuO-CeO_2 interface for the mixed systems, a relevant factor in the WGS as discussed in the introduction part.

Raman Spectroscopy

Raman spectra of the prepared systems are depicted in Figure 2. All the ceria containing materials, showed a marked band *ca.* 460 cm^{-1} which correspond to the triple degenerate F_{2g} mode of fluorite, the only one permitted in the first order [27]. Within the supports (Figure 2A) the Raman spectra of the Cu/Al sample matches well that of the CuO reference. Cupric oxide belongs to the C^6_{2h} space group with two molecules per primitive cell and presents 3 main active Raman modes $A_g + 2B_g$. In this sense, we can assign the peak at 288 cm^{-1} to the A_g mode and the peaks at 336, 620 cm^{-1} to the B_g modes [28]. In addition to the three bands, a broad band centred at 1150 cm^{-1}, assigned to multi-phonon (MP) transition was observed [29].

As for the Ce-Cu mixed supports, these copper modes are attenuated and a new band extended from 500 to 660 cm^{-1} is observed. This Raman mode which has been related to the presence of oxygen vacancies [30, 31] shows increasing relative intensity upon increasing the amount of Cu. This observation indirectly supports incorporation of copper into the fluorite cell in good agreement with the XRD data since the substitution of Ce^{4+} by Cu^{2+} is accompanied by the generation of oxygen vacancies ($Ce^{4+} + O^{2-} \leftrightarrow Cu^{2+} + O_v$; O_v being a doubly ionized oxygen vacancy) [16]. However, this broad band could also account for the presence of Cu_2O species that present some Raman active modes in this region of the spectra [32, 33]. Therefore the most likely situation is the overlapping of Cu_2O bands with the oxygen vacancies (O_v) ones as intended when this zone is analysed in details (Figure 2B). Similar circumstances reflecting close interaction between CeO_x –Cu_2O species were observed by STM upon dosing Ce to a Cu (111) single crystal [15] On the other hand, the small band centred at 269 cm^{-1} confirms the tetragonalization of the cubic structure by the presence of Ce^{3+} species, which indirectly support the formation of oxygen vacancies in the mixed systems. A similar behaviour was observed

elsewhere for Ce-Cu mixtures being Cu^{2+} the interchanging ion that gets into the ceria lattice [34]. Hence it seems that both Cu_2O and CuO species may coexist due to the ability of ceria to donate or accept electrons stabilizing the copper species.

The addition of gold (Figure 2C) introduces some fluorescence to the spectra. Interestingly, the intensity of the ceria F_{2g} mode decreases with the introduction of Cu, a fact that can be related to an increased optical absorption [16]. Also this band is slightly shifted and presents different shape for the Cu-containing samples indicating a strong Ce-Cu contact. Additionally the intensity of the Raman band at 500 to 660 cm^{-1} decreases when compared to the supports although the band remains present. The latter is an indication of preferential nucleation of gold in the oxygen vacancies of ceria [34].

UV-Vis spectroscopy

Deeper information about the electronic features of the studied materials was obtained by UV-Vis spectroscopy. Figure 3A shows the spectra of the supports. All the ceria based materials present charge transfer from 2p valence band of O^{2-} to 4f band of Ce^{4+} [35]. For the Ce-Cu mixed systems, widening and shifting of the absorption edge is observed, generally evidencing Ce-Cu interaction in fair agreement with the Raman and XRD data. Indeed the presence of copper introduces a second contribution in the 200-350 nm range due to the charge transfer band from O^{2-} to 3d band of Cu^{2+} as clearly seen in the spectra of the Cu/Al sample [36]. This sample also displays the typical broad band ascribed to the d-d transitions in the 500-800 nm zone [36].

Furthermore, a marked effect of Cu on ceria electronic properties is derived from the ceria band gap calculation (Table 2). A sequential drop in the band gap was observed upon increasing the copper loading on the mixed oxide, a trend that was also obtained for the gold based catalysts. Such a band gap contraction was previously attributed to the fluctuation of the potential energy caused by the spatial dependence of the local density of states in doped semiconductors [37]. In our particular situation Cu^{2+} is a d^9 cation with some capacity to accept electrons via back-bonding interaction. It is plausible that Cu unoccupied orbitals lay between the frontiers orbitals (HOMO-LUMO) of ceria, thus provoking the band gap contraction.

Gold deposition introduces a new absorption band with maximum in the range 550-600 nm. This contribution is assigned to the plasmon resonance of the gold nanoparticles [38]. It is should be noticed as well, that this gold plasmon absorption overlaps with Cu d-d transitions bands thus for the high Cu loading it is difficult to distinguish among both contributions. The effect of gold on the ceria band gap is also worth to mention. As indicated in table 2, gold leads to a systematical band gap decrease for the gold catalysts when compared to their parent supports. Somewhat this effect evidences a remarkable electronic metal-support interaction (EMSI). This electronic contact between Au and the multicomponent support controls the electronic state of the catalysts' surface thus influencing the ability of the catalysts to bond adsorbates and finally affecting the catalytic activity [39]

Reducibility: H_2-TPR

Temperature programmed reduction studies were conducted in order to study the redox properties of the catalysts and to analyze the interaction between the different metallic and oxide

species. For the supports (Figure 4A) the reduction of ceria and copper oxide were evidenced. For example, the Ce/Al material presents a broad reduction zone between 400-700 ^{0}C associated to the ceria surface reduction and a second late reduction process taking place around 900 ^{0}C which accounts for the ceria bulk reduction as reported elsewhere [40]. On the other extreme of the series the Cu/Al sample only displayed one reduction zone centered at 210 ^{0}C which corresponds to the copper oxide reduction process happening in one single step ($CuO + H_2 \rightarrow Cu + H_2O$) [41] Regarding the mixed systems, they reflect an intermediate reducibility behavior. For instance for the high ceria loading (Ce8Cu/Al) the profiles resembles that of the Ce/Al however both surface and bulk ceria reduction processes are shifted to lower temperatures due to the intimate Ce-Cu contact and also to the contribution of CuO reduction at low temperatures. On the other hand, Ce2Cu8/Al exhibits a similar profile to that of Cu/Al pointing that copper reduction is the dominant process. As for the Ce5Cu5/Al support the reduction of both CuO and CeO_2 take places simultaneously in an intermediate temperature window 250-350 ^{0}C.

The addition of gold shifts ceria surface reduction and, to a lesser extent, bulk reduction towards lower temperatures, an effect especially notable for the ceria rich samples, Ce/Al and Ce8Cu2/Al. In the case of Au/Ce5Cu5/Al the presence of gold splits the low temperature peak observed in the support into two peaks. Very likely the lower temperature one (centered at 180 ^{0}C) accounts for the reduction of CuO while the peak at 240 ^{0}C would correspond to ceria surface reduction. Also a small contribution of bulk reduction of ceria shows up. For Au/Ce2Cu8/Al the effect of gold is not so notorious and only a slight shift in the reduction temperature is observed. Finally the Au/Cu/Al present a more complex profile compared to its Cu/Al parent support. Several shoulders lying within the main reduction peak appeared, probably indicating different type of CuO particles in contact with gold. For instance, different copper

particle sizes and/or copper oxide structure (since according to Raman the presence of Cu_2O could not be discarded). Such shoulders are not envisaged when ceria is present which indicates a more homogenous copper reduction in the presence of ceria underlining the importance of the CuO-CeO_2 interaction in the redox properties. In any case, the overall effect is a promotion of the catalysts reducibility due to the presence of gold since normally gold facilitates the mobility of H_2 on the surface enhancing the catalyst components reduction [42]

Oxygen Storage Capacity

The water gas shift reaction is a redox process and therefore any suitable WGS catalyst must present excellent redox properties. In this sense, the OSC provides a precise idea of the catalysts' oxygen mobility. More concretely, OSC informs about the most reactive and most available oxygen atoms that in end are always ready to take part in the catalytic process [22]. It should be mentioned that the CO_2 formed in the OSC experiment is assumed to come only from the interaction between CO and the lattice oxygen from the catalysts. The presence of the WGS is discarded since no hydrogen was observed during the pulses experiments. Figure 5A shows the storage capacity of the studied supports at relevant temperatures for the WGS. As a general trend, the OSC increases with temperature for all the solids. Cu/Al and Ce/Al present comparable OSC values while all the Ce-Cu mixed systems exhibit rather higher oxygen storage capacity compared to the unmixed systems. In other words, a remarkable improvement of the oxygen mobility is achieved with the multicomponent CeO_2-CuO/Al_2O_3 catalysts. This effect mirrors the Cu-Ce synergy as a key factor influencing the catalyst's properties and backs up the discussion derived from Raman and XRD in terms of intimate Ce-Cu cooperation. It is worth mentioning that the Ce5Cu5/Al sample (the middle composition) leads to the best OSC results. Another interesting issue is that the OSC improvement is more marked in the lowest studied temperature.

Furthermore, the OSC showed by our systems are considerably superior to that published in previous work dealing with ceria and ceria-promoted materials [43]. In fact, this result is a consequence of the dispersion of ceria over a high surface carrier as alumina. This type of catalysts configuration allows higher surface to volume ratio and permits the mobility of oxygen not only from the surface but also from the bulk of the oxide [44].

The addition of gold boosted the OSC for the studied systems at all considered temperatures (Figure 5B). Such an oxygen mobility promotion agrees with the enhanced reducibility discussed in the TPR section and supports the presence of the so called EMSI effect. As proposed for a Ce-Fe mixed oxide the presence of added metal as Cu favors delocalizing the cerium $4f^1$ electrons through Ce(Cu)– O(V_O)–Ce(Cu) orbitals modifying the electronic density of gold as well as the dielectric properties of the ceria-copper mixed support [45]. This assumption agrees with Frost's junction proposal [46] in which the electron produced by ionizing the O vacancies of a semiconductor oxide is delocalized between the oxide conduction band states and the available Fermi levels in agreement with our UV-Vis data. The overlapping of the orbitals favors the electronic interchange processes among the constituents of the multicomponent catalysts accounting for promoted redox properties. In parallel, the addition of gold changes the trend within the series converting the samples richer in Cu into the most interesting materials in terms of OSC. The presence of Au weakens the M-O bond of the support due to the electronic transfer between the mixed oxide and the noble metal thus enhancing oxygen lability. In addition, the presence gold particles may act as channel for oxygen migration and storage on the support providing a second route for oxygen mobility [22]. Therefore the magnitude of Au-support interaction may affect to the OSC and it seems that the Au/Ce2Cu8/Al sample presents the strongest Au-mixed oxide contact as reflected by the lowest band gap and the highest OSC.

WGS behavior

Figure 6 shows the catalytic screening in the WGS reaction of the prepared materials. The activity of the supports is presented in Figure 6A. It is interesting to note that none of the supports reached high CO conversions being the ceria-rich samples the ones exhibiting poorer activity. However, the WGS performance progressively increases upon increasing the Cu loading. This result mainly reflects the behaviour of Cu/CuO_x as an active phase in the shift reaction. Indeed the Cu/Al sample is one of the most active supports only outweighed by the mixed Ce2Cu8/Al which reaches better conversions. It is therefore clear that small amounts of ceria benefits the activity of Cu in good agreement with the discussion derived from the OSC and Raman data. Cerium oxide provides oxygen vacancies which are highly reactive points for H_2O activation while motivates the oxygen mobility among the CeO_{2-x}/Cu interface sites favouring the CO oxidation process.

In any case, the conversions displayed by the supports are far from the thermodynamic limits making necessary the presence of gold. The WGS activity of the prepared gold catalysts is depicted in Figure 6B. Herein, a Au/Al catalysts is included for comparison. This sample is hardly active in the whole temperature window indicating that despite gold is fundamental to reach high CO conversions, it requires the presence of an active support with oxygen mobility to actually work. Indeed, as postulated by Rodriguez and co-workers gold cannot develop any water splitting which is the rate controlling step in the shift reaction and therefore it mandatorily need the support assistance to carry out water activation [47]. Our data clearly supports this theory, since all the ceria containing materials are rather active. It seems that Au/Ce/Al is the least active among the multicomponent catalysts although this solid is more active than any of the $Ce_xCu_{1-x}O_2/Al_2O_3$ supports remarking the role played by gold. The sequential inclusion of

copper in the catalyst's formula leads to a pronounced improvement to the WGS activity. Indeed, the richer copper compositions Au/Ce2Cu8/Al and Au/Cu/Al displayed the highest CO conversion within the series, both of them showing a rather good shift activity especially at low temperatures. Actually these samples exhibited the greatest OSC confirming the correlation between the oxygen mobility and the activity in a redox process such as WGS. Furthermore, despite their parent supports were the most active ones, elevated CO conversions are only reached when gold is present. In other words, the three components Au, Cu and CeO_2 acting cooperatively are required to achieve an enhanced WGS behaviour.

For the gold based catalysts, it seems that copper loading is the most important factor guiding the catalytic performance. The beneficial effect of copper in the shift activity is a result of several factors happening at same time due to the complex nature of the catalysts. For the medium and low Cu loadings, the incorporation of Cu to the ceria lattice evidenced by XRD increases the oxygen vacancies population on ceria (as shown in the Raman spectra of the Ce5Cu5/Al solid). As demonstrated by Tabakova et al. the concentration of these punctual defects is directly related to the WGS activity in Au/CeO_2 based catalysts [48]. For instance when a redox mechanism is considered as dominant in the WGS as previously demonstrated [49, 50], oxygen vacancies are viewed as the activation points to initiate the water splitting. Indeed an oxygen defect in the oxide lattice is the perfect place to anchor water since in the end an oxygen atom (from the water) is occupying the void space left by another oxygen (the lattice oxygen). Furthermore the mixed systems are materials with enhanced reducibility and fairly good oxygen mobility, which in turns drives to better CO oxidation capabilities [52]. Alternatively if the "formate associative mechanism" is playing a role as proposed elsewhere [50-53] the formate decomposition towards CO_2 and H_2 is the rate controlling step. In this sense, the boosted activity displayed by the mixed

systems should be related to the lower energy barrier to decompose this intermediate when Au, Cu and CeO_2 act synergistically. Indeed similar activity promotion was found for a Pt/ $Ce_{1-x}La_xO_{2-\gamma}$ system for which the Ce/La ratio controls the activity due to the creation of higher amount of active sites in the metal-support interface [11]. In our case the activity is controlled by the Ce/Cu ratio and in good agreement with ref. [11] the best performance was obtained for the sample with the lowest band gap evidencing the importance of the Au-mixed oxide contact.

For the higher copper loadings, the activity is a consequence of their elevated OSC, but also to the obvious contribution of Cu as an additional active phase in the WGS. According the TPR the reduction of CuO to Cu is expected to occur in the WGS environment leading to a system with two metals Au and Cu supported on alumina in the case of Au/Cu/Al and ceria alumina for the Au/Ce2Cu8/Al. Differently to Au, Cu may carry out the water splitting itself. As shown by DFT calculations, the first and the most energy-consuming step, for a single crystal of Cu (100), is water dissociation which is slightly endothermic (+0.39 eV) with an energy barrier of +1.13 eV [3]. In the case of Au (100) this step is even more endothermic (+0.74 eV) and the corresponding barrier is also higher (+1.53 eV) [3] in good concordance with our activity data since the Au/Al sample is hardly active while Cu/Al presents moderate activity (Figure 6A and 6B).

The high activity of copper species in the WGS reaction may masque the effect of ceria since under a WGS model mixture Au/Cu/Al and AuCe2Cu8/Al behaves similarly. Nevertheless some interesting differences appear when the WGS test is developed under a realistic WGS stream as presented in Figure 7. As shown in the plot, the CO conversion in a surrogate post reforming mixture is shifted towards higher temperatures. The lower activity of the catalysts under this mixture is related to a shift in the equilibrium as a consequence of Le Chatelier principle. Also CO_2 and H_2 may compete with H_2O and CO for the active sites of the catalysts reducing the

chances for the WGS. In any case, only the catalyst containing ceria reaches equilibrium conversion in the studied range. Despite the activity is mainly controlled by the copper concentration, the presence of ceria is critical to achieve the best performance. In fact, Wang et al. reported a synergistic Cu-ceria O vacancy interaction as a key factor in the WGS activity [54]. This interaction enhances the chemical activity of Cu, and the presence of Cu facilitates the formation of O vacancies in ceria under reaction conditions in good agreement with our OSC and Raman data. Such a situation provides more active sites for water dissociation.

In order to validate the efficiency of our catalysts their activity should be compared to reference catalysts published in literature. In this sense, Table 3 presents the CO conversion of our best catalysts in the low and the high temperature range compared to the conversion exhibited by some highly active Au-CeO_2 and CuO-CeO_2 catalysts in literature. For a more accurate comparison we have selected a number of catalysts tested under the same WGS mixture (4.5% CO + 30% H_2O balance in inert gas) and same GHSV (4000 h^{-1}). As shown in Table 3 our best catalysts outperform the activity presented by typical Au/CeO_2 and CuO-CeO_2 catalysts previously published. The differences are especially relevant at low temperature where only the commercial formulation (CuO-ZnO-Al_2O_3) reported in ref. [58] presents comparable conversion to that achieved by AuCe2Cu8/Al and Au/Cu/Al. This approximated comparison confirms the promising performance of the developed multicomponent catalysts for the WGS reaction.

Stability tests

Further differences can be established when the stability of the catalysts is studied. Figure 8 presents the long-term stability test of the most active samples. The test was carried out at

medium conversion to ensure conditions far from the equilibrium. As shown in the plot, the Au/Cu/Al catalyst undergoes a progressive activity drop from 43 to 30 % of CO conversion after 72 hours of continuous operation. On the hand, Au/Ce2Cu8/Al catalyst also loses activity during the first 40 hours of reaction but in a minor extent. After that, the system seems to reach the steady state maintaining a stable conversion during the rest of the test.

For a practical application in the field of the hydrogen technology all the catalysts involved in the fuel processor must tolerate the start-up/shut-down cycles of the engine. This is a rather severe stability test since during the stop stages the reactor is cooled down at room temperature with the reactive mixture flowing through the catalytic bed. The later involves that liquid water may condensate on the catalysts´ porous eventually deactivating the system. In our case some curious result were obtained as shown in Figure 9. Apparently, the Au/Cu/Al catalyst does not tolerate the cycling situations suffering for a clear deactivation after a series of consecutive cycles. On the other hand, the Au/Ce2Cu8/Al catalysts successfully withstand the start/stop operations with no evidence of activity depletion. This is a rather promising result in terms of applicability especially when portables applications are envisaged.

In summary, the multicomponent catalysts containing ceria (Au/Ce2Cu8/Al) is more stable in both long term situations and start-up/shut-downs tests. The presence of ceria seems therefore to be indispensable. The reasons behind this superior stability are beyond of the aims targeted in this work. However, it can be argue that the ceria helps to mitigate the typical catalysts deactivation due to carbonaceous species formation. It is plausible that the carbonate-like species form during WGS would be further decomposed to CO_2 due to the great oxygen mobility of this sample. Additionally, oxygen vacancies presented in ceria allows greater gold and copper dispersion and the strong Au-O vacancy / Cu-O vacancy contact guarantees a good metallic

phase anchoring in the surface avoiding any sintering phenomena. TPD experiments to evaluate the stability of the carbonaceous species formed in the WGS. The spent samples after the transient start/stop tests were investigated and the results are presented in Figure 10 (new figure in the revised version). In order to validate this hypothesis TPD experiments of the spent samples in the start/stop test were conducted (Figure 10). As shown in the figure the CO_2 desorption profiles are rather different in the presence and the absence of ceria. For the ceria containing catalyst the CO_2 is desorbed before 400 ^{o}C. On the other hand, the Au/Cu/Al sample presents three process of CO_2 desorption probably associated to three types of carbonaceous species formed during the WGS. The strongest desorption process takes place between 400 and 700 ^{o}C which indicates a high stability of the formed carbonaceous species. This result reinforces the idea that ceria helps to avoid the formation carbonates-like blocking species that are related to the catalyst's deactivation making the AuCe2Cu8/Al catalyst more stable than the Au/Cu/Al one.

Conclusions

A new family of multicomponent $Au/Ce_{1-x}Cu_xO_2/Al_2O_3$ catalysts for the WGS reaction is proposed in this work. The properties of the prepared materials are greatly influenced by the Ce/Cu ratio. The mixed system exhibit a marked Ce-Cu synergy together with a strong Au-support interaction which modulates the key features controlling the activity such as oxygen vacancies population, catalyst's reducibility and oxygen storage capacity.

Even though copper is an active phase in the WGS, the presence of Au is crucial to achieve elevated performance. This cooperative Au-Cu effect also rules the other way round: among the gold catalysts, the better catalytic results are obtained for rich copper compositions. Moreover,

the presence of ceria is indispensable for an optimum performance and greater stability. Ceria containing catalysts seems to form less stable carbonaceous species during the reaction. Furthermore, ceria enhances the chemical activity of both gold and copper by providing oxygen vacancies while copper and gold facilitate ceria redox cycling, leading to a triple synergy among Au, Cu and CeO_2. In the best situation our complex catalysts displayed high activity under realistic WGS reaction conditions with a fairly good stability in continuous and interrupted operations, a desirable issue for mobile or static applications.

Overall, this works provides some guidelines for a reasonable design of efficient WGS catalysts while trying to discern the reason under the displayed performance. It seems that both structural and electronic perturbations arising from the combination of several active phases must be carefully tailored to achieve the best activity/stability commitment.

Acknowledgements

Financial support for this work has been obtained from Junta de Andalucía (TEP-8196) and from the Spanish Ministerio de Economía y Competitividad (ENE2012-374301-C03-01 and ENE2013-47880-C3-2-R) co-financed by FEDER funds from the European Union. T.R. Reina acknowledges CSIC for his JAE-Predoc fellowship.

References

[1] G.C. Bond, C. Louis, D.T. Thompson, in: G. H. Hutchings (Ed), Catalysis by Gold, Imperial College Press, London 2006, vol. 6.

[2] B. Hammer, J.K. Nørskov, Nature 376 (1995) 238-240.

[3] J.A. Rodriguez, Catal. Today 160 (2011) 3-10.

[4] G.C. Bond, D.T. Thompson, Catal. Rev. Sci. Eng. 41 (1999) 319-388.

[5] R. Si, M. Flytzani-Stephanopoulos, Angew. Chem. Int. Ed. 47 (2008) 2884-2887.

[6] M. Haruta, M. Daté, Appl. Catal. A 222 (2001) 427-437.

[7] A. Stephen, K. Hashmi, G.J. Hutchings, Angew. Chem. Int. Ed. 45 (2006) 7896- 7936.

[8] G.J. Hutchings, J. Catal. 96 (1985) 292- 295.

[9] D. Andreeva, V. Idakiev, T. Tabakova, A. Andreev, J. Catal. 158 (1996) 354-355.

[10] T.R. Reina, M. Gonzalez-Castano, S. Palma, S. Ivanova, J.A. Odriozola, in: Z. Ma and S. Da (Eds) Heterogenous gold catalysts and catalysis, RSC catalysis book series, 2014 Vol 18. 111-139.

[11] K.C. Petallidou, A.M. Efstathiou, Appl. Catal. B 140-141 (2013) 333-347.

[12] Q. Fu, H. Saltsburg, M. Flytzani-Stephanopolous, Science 310 (2003) 935-938.

[13] P. Panagiotopoulou, J. Papavasiliou, G. Avgouropoulos, T. Ioannides, D.I. Kondarides, Chem. Eng. J. 134 (2007) 16-22.

[14] M. Boaro, M. Vicario, J. Llorca, C. de Leitenburg, G. Dolcetti, A. Trovarelli, Appl.

Catal. B 88 (2009) 272-282.

[15] J.A. Rodriguez, J. Graciani, J. Evans, J.B. Park, F. Yang, D. Stacchiola, S. Senanayake, S. Ma, M. Pérez. P. Lui, J. Fdez. Sanz, J. Hrbek, Angew. Chem. Int. Ed. 48 (2009) 8047-8050.

[16] D. Gamarra, G. Munuera, A.B. Hungria, M. Fernandez-Garcia, J.C. Conesa, P.A. Midgley, X.Q. Wang, J.C. Hanson, J.A. Rodriguez, A. Martinez-Arias, J. Phys. Chem. C 111 (2007) 11026-11038.

[17] Y. Li, Q. Fu, M. Flytzani-Stephanopoulos, Appl. Catal. B 27 (2000) 179-191.

[18] L. Pastor-Pérez, T.R. Reina, S. Ivanova, M.A. Centeno, A. Sepulveda-Escribano, J.A. Odriozola, Catalysts 5 (1) (2015) 298-309.

[19] T.R. Reina, S. Ivanova, M.A. Centeno, J.A. Odriozola, Catal. Today 253 (2015**)** 149-154.

[20] S. Ivanova, C. Petit, V. Pitchon, Appl. Catal. A 267 (2004) 191-201.

[21] S. Kacimi, J. Barbier, R. Taha, D. Duprez, Catal. Lett. 22 (1993) 343-350.

[22] S. Bedrane, C. Descorme, D. Duprez, Catal. Today 75 (2002) 401-405.

[23] S. Ivanova, V. Pitchon, C. Petit, J. Mol. Catal. A: Chem. 256 (2006) 278-286.

[24] F. Moreau, G.C. Bond, Appl. Catal. A 302 (2006) 110-117.

[25] X. Wang, J.A. Rodriguez, J. Phys. Chem. B 109 (2005) 19595-195603.

[26] X. Liao, W. Chu, X. Dai, V. Pitchon, Appl. Catal. B. 142 (2013) 25-37.

[27] J.E. Spanier, R.D. Robinson, F. Zhang, S.W. Chan, I.P. Herman, Phys. Rev. B 64 (2001) 245407/1–8.

[28] J.F. Xu, W. Ji, Z.X. Shen, S.H. Tang, J. Solid State Chem. 147 (1999) 516-519.

[29] W. Wang, Q. Zhou, X. Fei, Y. He, P. Zhang, G. Zhang, L. Peng, W. Xie, Cryst. Eng. Comm 12 (2010) 2232-2237.

[30] J. R. McBride, K.C. Hass, B.D. Poindexter, W.H.J. Weber, Appl. Phys. 76 (1994) 2435-2441.

[31] H. Bao, X. Chen, J. Fang, Z. Jiang, W. Huang, Catal. Lett. 125 (2008) 160-167.

[32] P.Y. Yu, Y.R. Shen, Y. Petroff, Solid State Comm. 12 (1973) 973-975.

[33] P.F. Williams, S.P. Porto, Phys. Rev. 8 (1973) 1782-1785.

[34] O.H. Laguna, W.Y. Hernández, G. Arzamendi, L.M. Gandía, M.A. Centeno, J.A. Odriozola, Fuel 118 (2014) 176-185.

[35] V. Petrovsky, B.P. Gorman, H.U. Anderson, T. Petrovsky, J. Appl. Phys. 90 (2001) 2517-252.

[36] M.H. Groothaert, J.A. van Bokhoven, A. Battiston, B.M. Weckhuysen, R.J. Schoonheydt Am. Chem. Soc. 125 (2003) 7629-7640.

[37] T. Dhannia, S. Jayalekshmi, M.C. Santhosh Kumar, T. Prasada Rao, A. Chandra Bose, J. Phys. Chem. Solids 7 (2010) 1020-1028.

[38] N. Pestryakov, N. Bogdanchikova, A. Simakov, I. Tuzovskaya, F. Jentoft, M. Farias, A. Díaz, Surf. Science 610 (2007) 3792-3795.

[39] C.T. Campbell, Nature Chem. 4 (2012) 597-598.

[40] L. Pastor-Pérez, R. Buitrago-Sierra, A. Sepúlveda-Escribano, Int. J. Hydrogen Energ. 39 (2014) 17589-17599.

[41] M.F. Luo , P. Fang, M. He, Y. L. Xie J. Mol. Catal. A 239 (2005) 243–248

[42] S. Royer, D. Duprez, ChemCatChem, 3 (2011) 24-65.

[43] C.E. Hori, H. Permana, K.Y. Simon A. Brenner, K. More, K.M. Rahmoeller, D. Belton, Appl. Catal. B. 16 (1998) 105-117.

[44] T.R. Reina, S. Ivanova, J.J. Delgado, I. Ivanov, T. Tabakova, V. Idakiev, M.A. Centeno, J.A. Odriozola, ChemCatChem 6 (2014) 1401-1409.

[45] M. Gonzalez-Castano, T.R. Reina, S. Ivanova, M.A. Centeno J.A. Odriozola, J. Catal. 314 (2014) 1-9.

[46] J.C. Frost, Nature 334 (1988) 577-580.

[47] J.A. Rodriguez, S. Ma, P. Liu, J. Hrbek, J. Evans, M. Pérez, Science 318 (2007) 1757-1760.

[48] T. Tabakova, G. Avgouropoulos, J. Papavasiliou, M. Manzoli, F. Boccuzzi, K. Tencheva, F. Vindigni, T. Ioannides, Appl.Catal. B 101 (2011) 256-265.

[49] C.M. Kalamaras, S. Americanou, A.M. Efstathiou J. Catal. 279 (2011) 287–300.

[50] C.M. Kalamaras, I. D. Gonzalez, R. M. Navarro, J.L. G. Fierro, A.M. Efstathiou J. Phys. Chem. C (2011) 115 (23) 11595–11610.

[51] C. Ratnasamy, J. Wagner, Catal. Rev. 51 (2009) 325-440.

[52] R. Leppelt, B. Schumacher, V. Plzak, M. Kinne, R.J. Behm J. Catal. 244 (2006) 137-152.

[53] F.C. Meunier, D. Reid, A. Goguet, S. Shekhtman, C. Hardacre, R. Burch, W. Deng, M. Flytzani-Stephanopoulos J. Catal. 247 (2007) 277–287.

[54] X. Wang, J.A. Rodriguez, J.C. Hanson, D. Gamarra, A. Martínez-Arias, M. Fernández-García, J. Phys. Chem. B 110 (2006) 428-434.

[55] D. Andreeva, V. Idakiev, T. Tabakova a, L. Ilievaa, P. Falaras, A. Bourlinos, A. Travlos Catal. Today 72 (2002) 51–57.

[56] T. Tabakova F. Boccuzzi, M. Manzoli, J.W. Sobczak, V. Idakiev, D. Andreeva Appl. Catal. A 298 (2006) 127–143.

[57] Z.-Y. Yuan,V. Idakiev, A.Vantomme, T. Tabakova, T.-Z. Ren , B.-L. Su Catal. Today 131 (2008) 203–210.

[58] T. Tabakova, V. Idakiev, J. Papavasiliou, G. Avgouropoulos, T. Ioannides Catal. Comm. 8 (2007) 101–106.

Figure 1 XRD patterns of the prepared materials. A) supports; B) gold based catalysts.

Figure 2 Raman spectra of the synthesis solids. A) supports; B) oxygen vacancies zone; C) gold based catalysts.

Figure 3 UV-vis spectra. A) supports B) gold based catalysts.

Figure 4 H_2-TPR profiles. A) supports; B) Gold based catalysts.

Figure 5 Oxygen storage capacity (OSC) of the materials. A)supports; B) gold based catalysts.

Figure 6 catalytic screening in a model WGS mixture (30% H_2O + 4.5 % CO balanced in N_2) A) supports; B) gold based catalysts.

Figure 7 Catalytic activity under a post reforming WGS mixture.

Figure 8 Long term stability test

Figure 9 Start-up/shutdown stability testunder realistic conditions (50% H_2; 12% CO_2; 30% H_2O; 11% CO) after the long term stability test at 280 ^oC.

Figure 10 CO_2-TPD profiles of the spent catalysts after the start-up/shutdown test.

Table 1. Chemical composition, specific surface area, ceria crystallite sizeand ceria lattice parameter of the prepared catalysts.

Sample	CeO_2 (wt.%)	CuO (wt.%)	Al_2O_3 (wt.%)	Au (wt.%)	S_{BET} (m^2/g)	[2]CeO_2 crystallite size (nm)	[3]CeO_2 lattice parameter (Å)
[1]**Au/Al**	-	-	98.8	1.2	215	-	-
Au/Ce/Al	16.6	-	81.4	2.0	138	8.0	5.402
Au/Cu/Al	-	13.1	85.4	1.5	146	-	-
Au/Ce8Cu2/Al	15.8	1.6	80.5	2.1	130	7.3	5.398
Au/Ce5Cu5/Al	10.9	4.5	82.8	1.7	144	5.3	5.394
Au/Ce2Cu8/Al	4.9	7.5	85.9	1.6	140	6.6	5.406

[1]Further characterization details of the Au/Al sample can be found in ref. [44]
[2]average particles size, calculated from Scherrer's equation and (111) crystallographic plane
[3]unit cell parameter, calculated from using Bragg's equation for a cubic cell.

Table 2. Indirect ceria band gap

Sample	Band gap (eV) ±0.05
Ce/Al	3.11
Ce8Cu2/Al	2.98
Ce5Cu5/Al	2.87
Ce2Cu8/Al	2.61
Au/Ce/Al	3.01
Au/Ce8Cu2/Al	2.90
Au/Ce5Cu5/Al	2.82
Au/Ce2Cu8/Al	2.57

Table 3. CO conversion at 180 and 300 ^{0}C of the most active samples developed in this study compared to CO conversion of reference WGS catalysts in literature. All the samples has been tested under the same WGS mixture and space velocity

catalyst	CO conv. (%) at 180 ^{o}C	CO conv. (%) at 300 ^{o}C
Au/Ce2Cu/Al	68.2	96.1
Au/Cu/Al	66.1	94.3
1Au/CeO_2 [56]	16.2	88.1
3Au/CeO_2 [56]	32.0	91.0
CuCe-DP [57]	56.0	92.2
Au/CeO_2-M [58]	57.8	88.7
CuO/CeO_2 [59]	28.0	66.0
CuO-ZnO-Al_2O_3 [59]	68.0	91.2

Figure 1

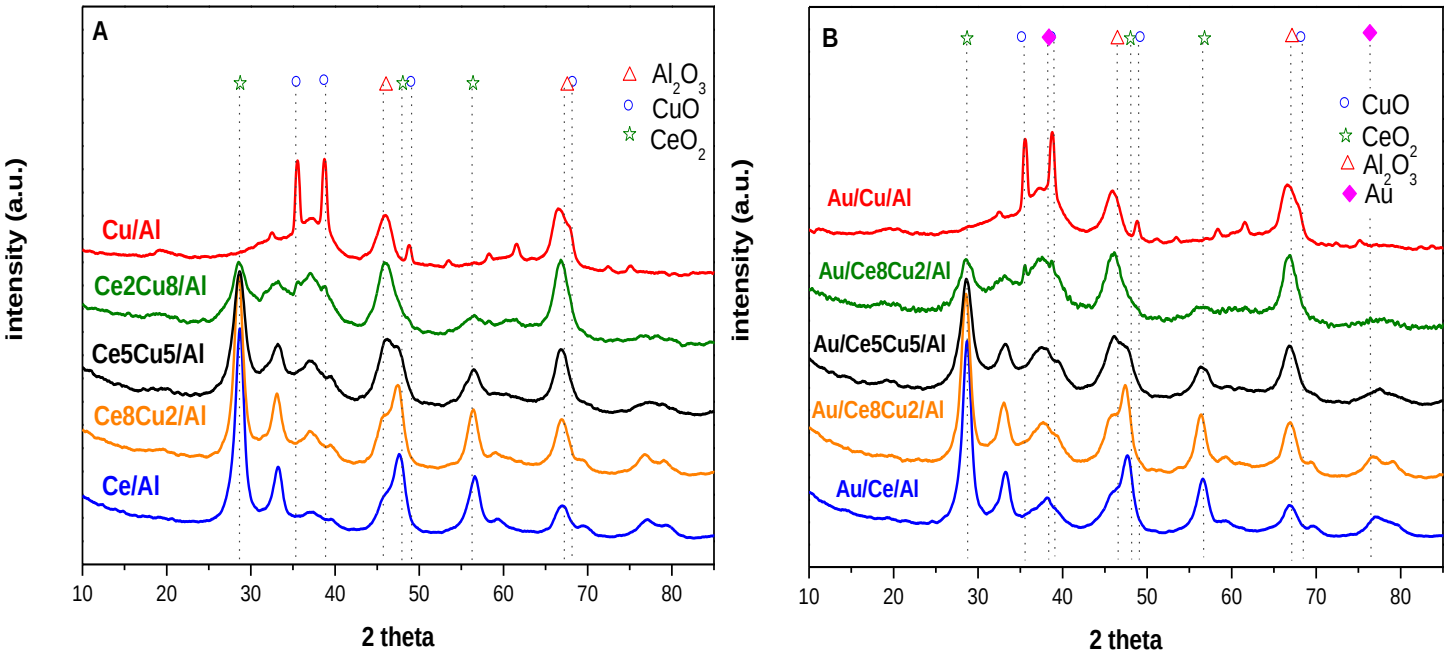
A
Al2O3
CuO
CeO2
Cu/Al
Ce2Cu8/Al
Ce5Cu5/Al
Ce8Cu2/Al
Ce/Al
intensity (a.u.)
10
20
30
40
50
60
70
80
2 theta
B
CuO
CeO2
Al2O3
Au
Au/Cu/Al
Au/Ce8Cu2/Al
Au/Ce5Cu5/Al
Au/Ce8Cu2/Al
Au/Ce/Al
intensity (a.u.)
10
20
30
40
50
60
70
80
2 theta

Figure 2

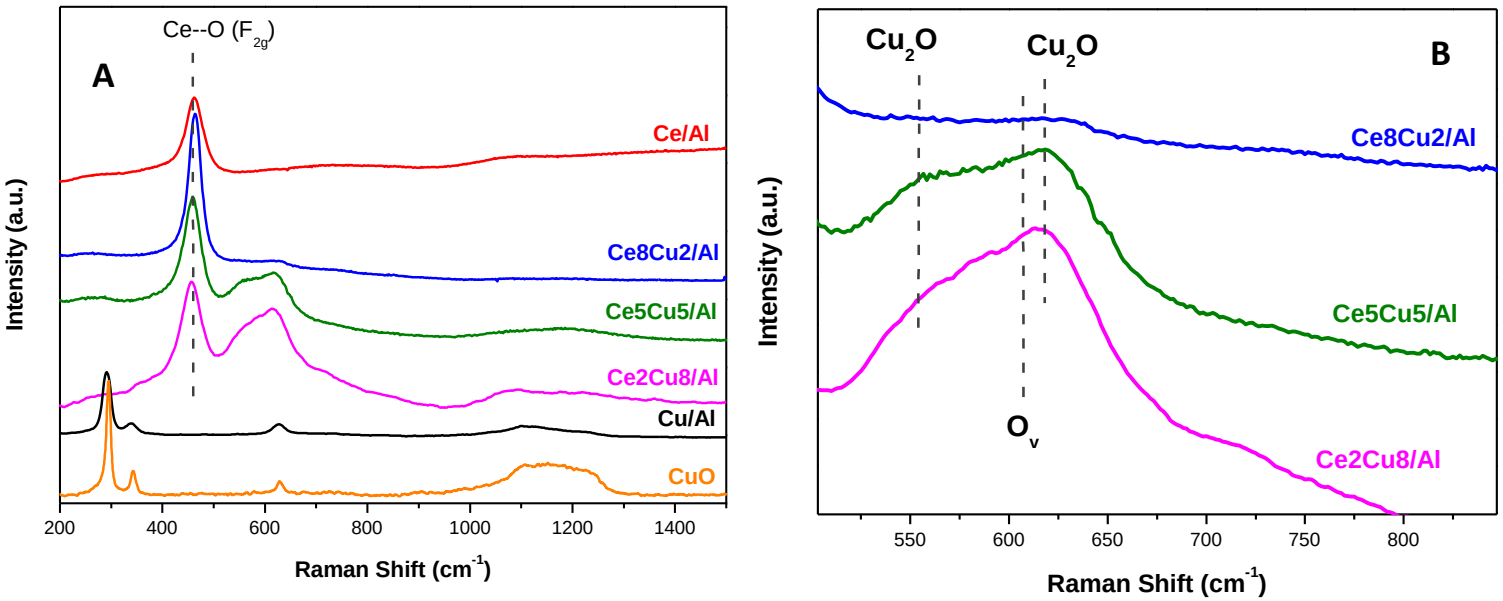
A
Ce--O (F_{2g})
Ce/Al
Ce8Cu2/Al
Ce5Cu5/Al
Ce2Cu8/Al
Cu/Al
CuO
Intensity (a.u.)
200
400
600
800
1000
1200
1400
Raman Shift (cm^{-1})
B
Cu_2O
Cu_2O
Ce8Cu2/Al
Ce5Cu5/Al
O_v
Ce2Cu8/Al
Intensity (a.u.)
550
600
650
700
750
800
Raman Shift (cm^{-1})

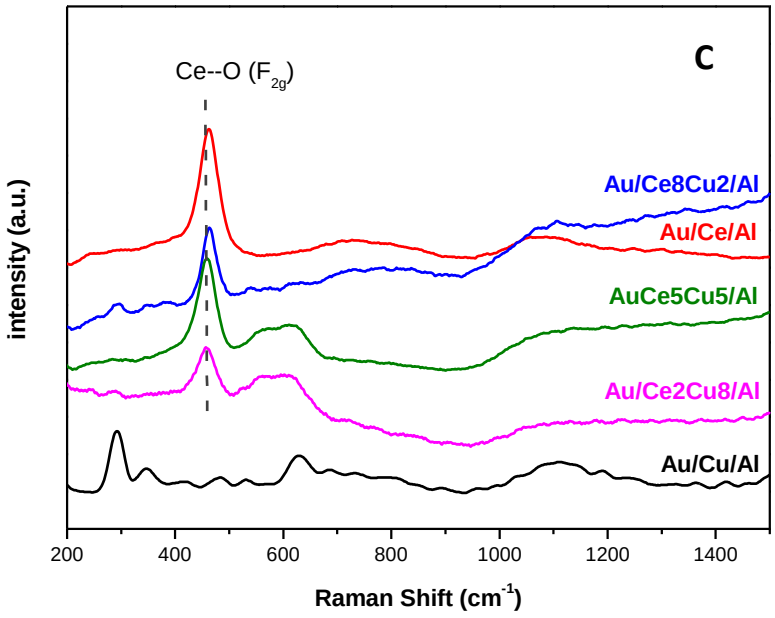
C
Ce--O (F_{2g})
Au/Ce8Cu2/Al
Au/Ce/Al
AuCe5Cu5/Al
Au/Ce2Cu8/Al
Au/Cu/Al
intensity (a.u.)
200
400
600
800
1000
1200
1400
Raman Shift (cm^{-1})

Figure 3

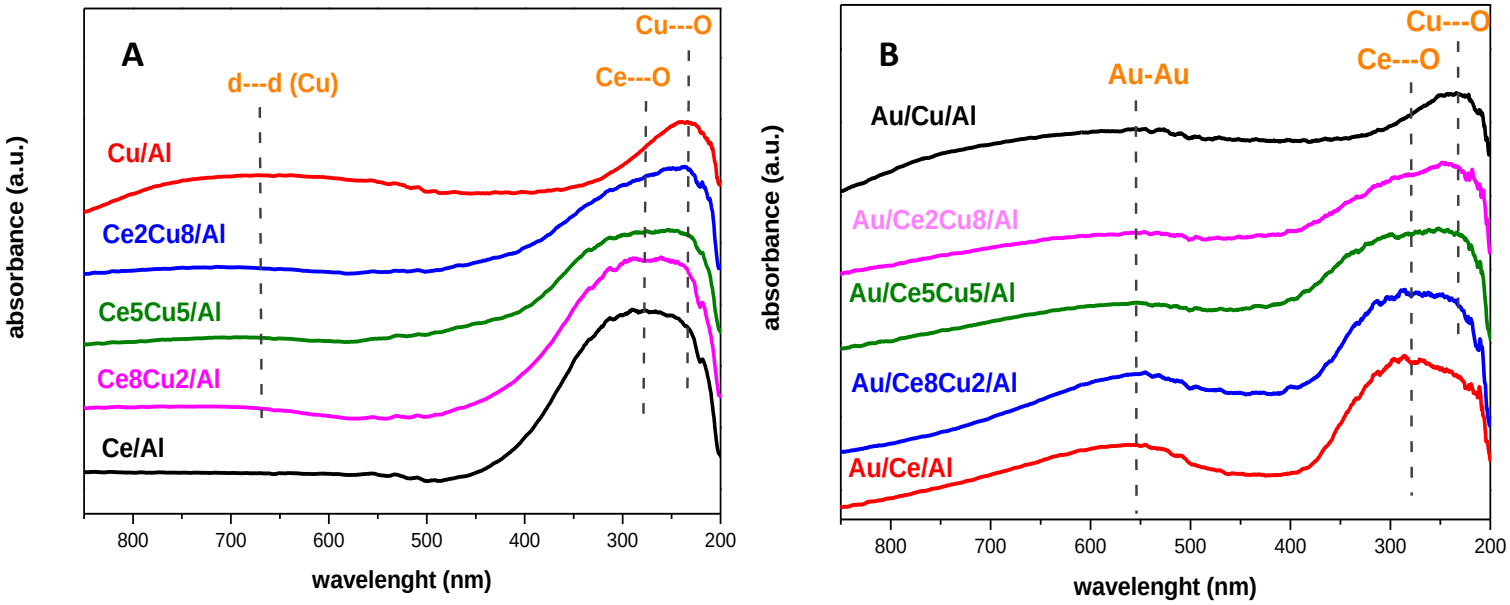
A
d---d (Cu)
Ce---O
Cu---O
Cu/Al
Ce2Cu8/Al
Ce5Cu5/Al
Ce8Cu2/Al
Ce/Al
absorbance (a.u.)
800
700
600
500
400
300
200
wavelenght (nm)
B
Au-Au
Ce---O
Cu---O
Au/Cu/Al
Au/Ce2Cu8/Al
Au/Ce5Cu5/Al
Au/Ce8Cu2/Al
Au/Ce/Al
absorbance (a.u.)
800
700
600
500
400
300
200
wavelenght (nm)

Figure 4

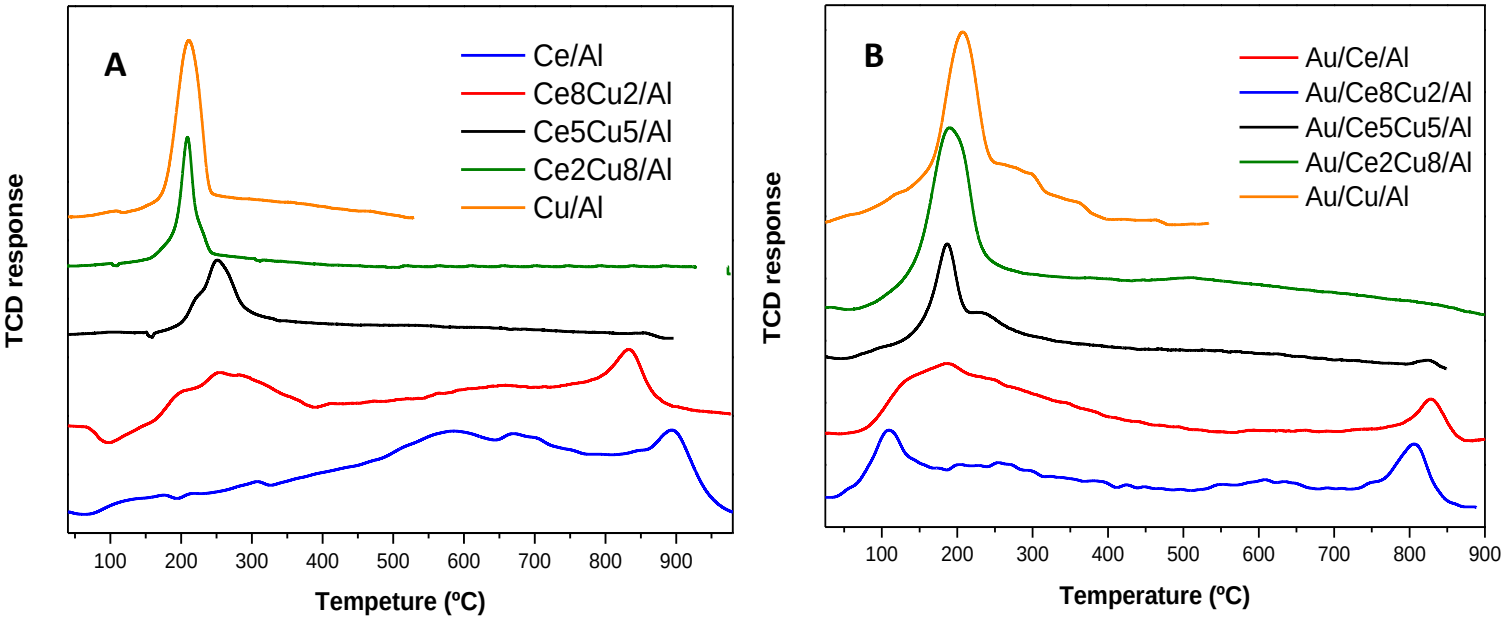
A
Ce/Al
Ce8Cu2/Al
Ce5Cu5/Al
Ce2Cu8/Al
Cu/Al
TCD response
100
200
300
400
500
600
700
800
900
Tempeture (ºC)
B
Au/Ce/Al
Au/Ce8Cu2/Al
Au/Ce5Cu5/Al
Au/Ce2Cu8/Al
Au/Cu/Al
TCD response
100
200
300
400
500
600
700
800
900
Temperature (ºC)

Figure 5

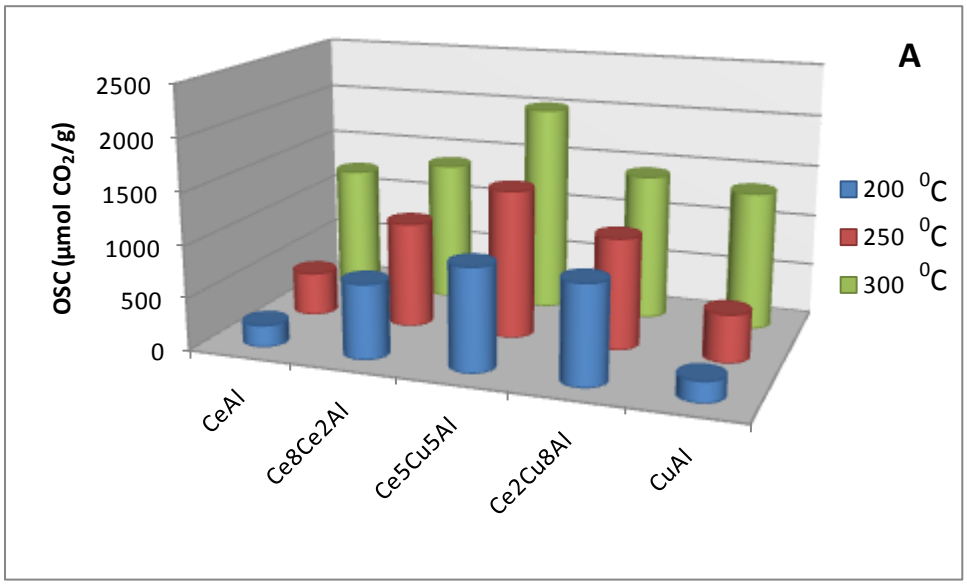
A
OSC (µmol CO_2/g)
2500
2000
1500
1000
500
0
CeAl
Ce8Ce2Al
Ce5Cu5Al
Ce2Cu8Al
CuAl
200 ^{0}C
250 ^{0}C
300 ^{0}C

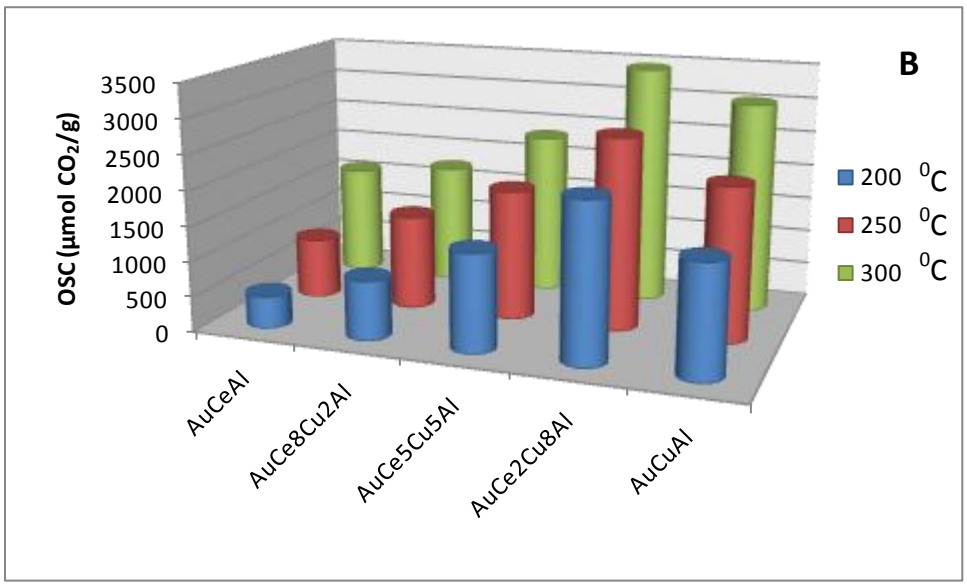
B
OSC (µmol CO_2/g)
3500
3000
2500
2000
1500
1000
500
0
AuCeAl
AuCe8Cu2Al
AuCe5Cu5Al
AuCe2Cu8Al
AuCuAl
200 ^{0}C
250 ^{0}C
300 ^{0}C

Figure 6

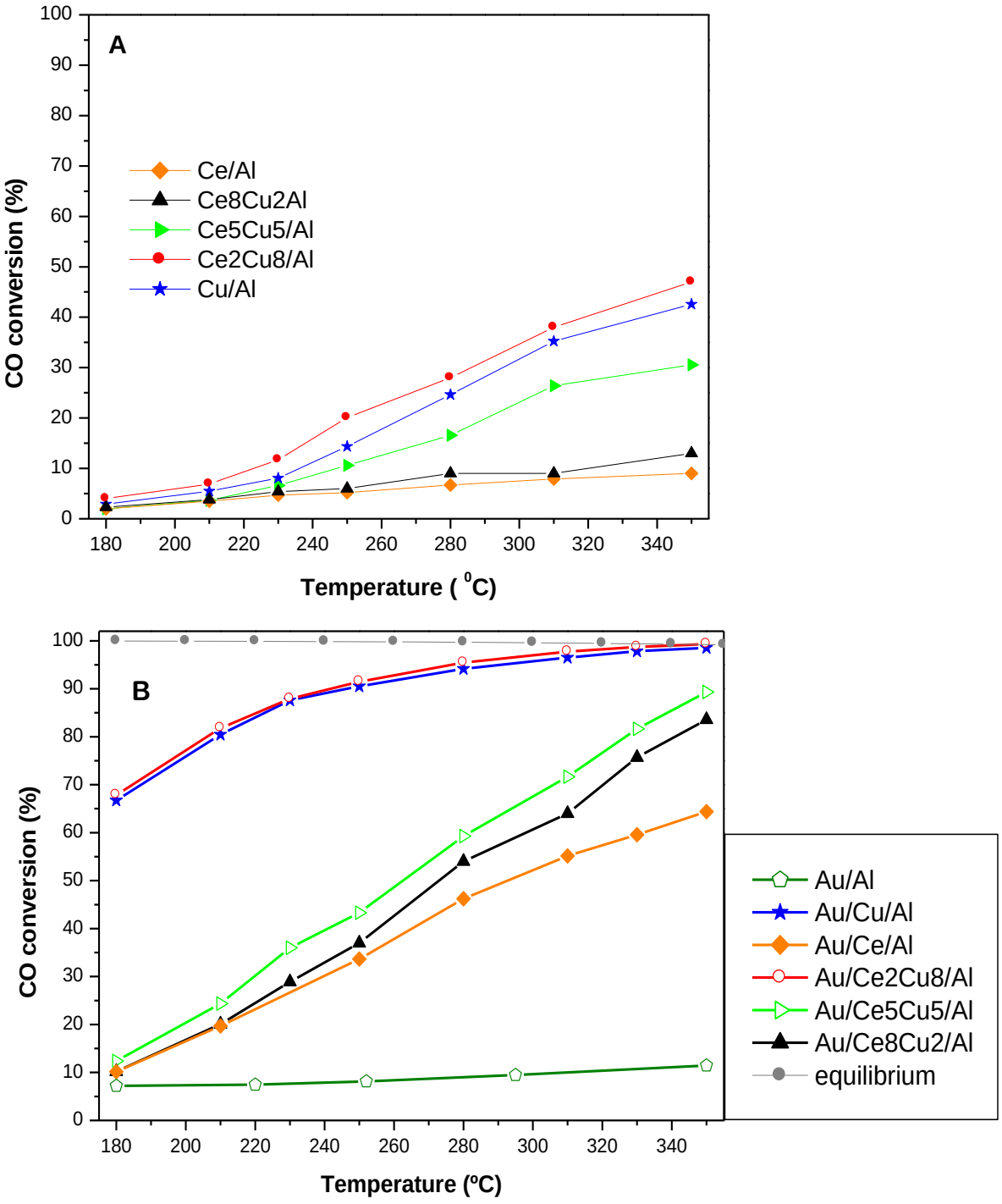
A
CO conversion (%)
Temperature (°C)
Ce/Al
Ce8Cu2Al
Ce5Cu5/Al
Ce2Cu8/Al
Cu/Al
B
CO conversion (%)
Temperature (°C)
Au/Al
Au/Cu/Al
Au/Ce/Al
Au/Ce2Cu8/Al
Au/Ce5Cu5/Al
Au/Ce8Cu2/Al
equilibrium

Figure 7

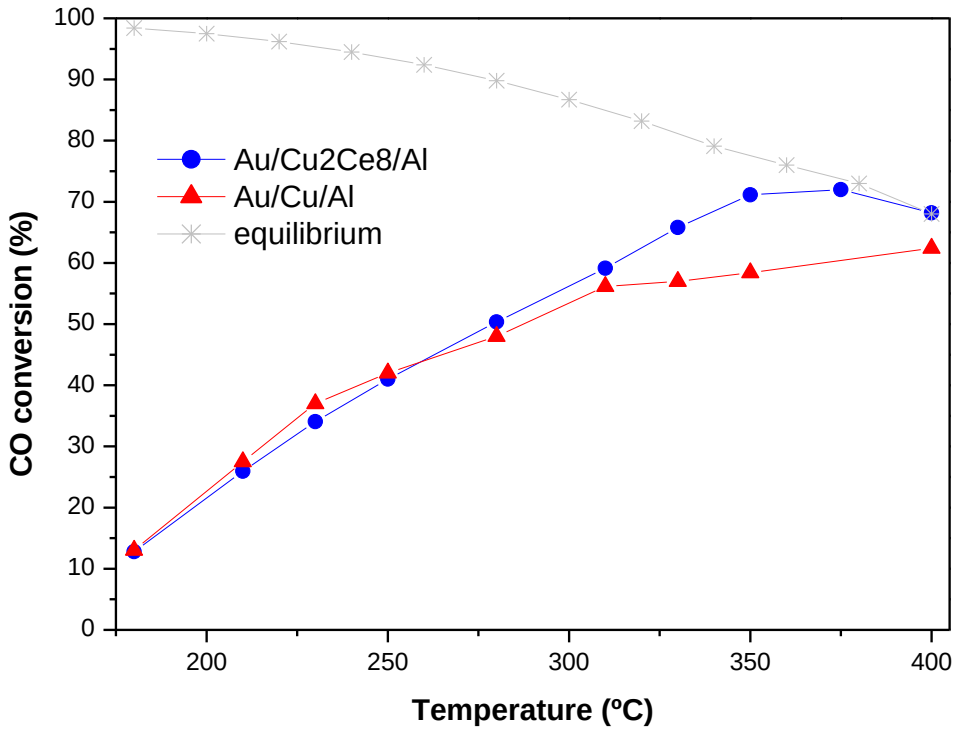
100
90
80
70
60
50
40
30
20
10
0
200
250
300
350
400
CO conversion (%)
Temperature (ºC)
Au/Cu2Ce8/Al
Au/Cu/Al
equilibrium

Figure 8

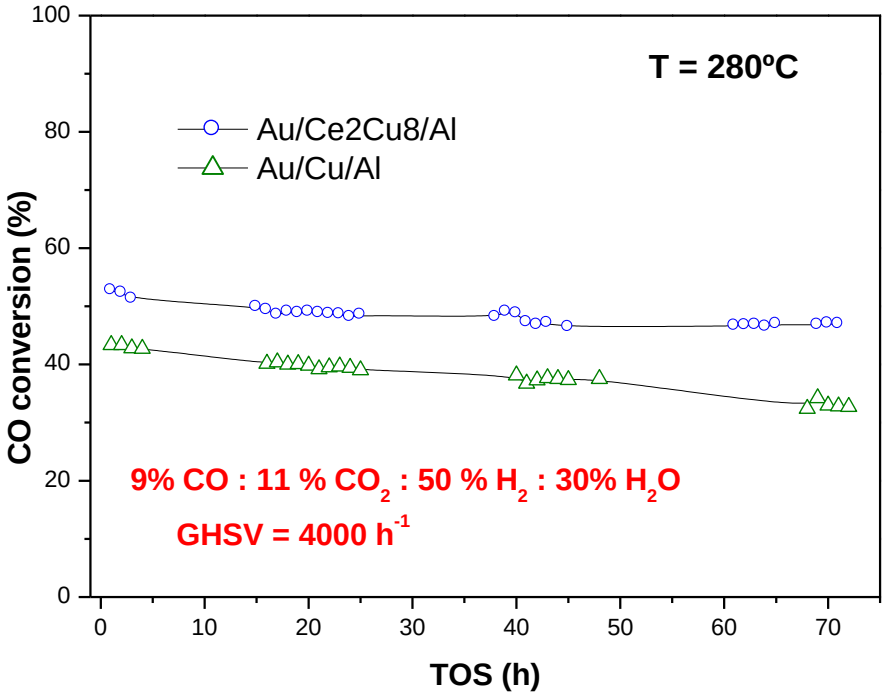
T = 280ºC
Au/Ce2Cu8/Al
Au/Cu/Al
CO conversion (%)
TOS (h)
9% CO : 11 % CO2 : 50 % H2 : 30% H2O
GHSV = 4000 h-1
0
20
40
60
80
100
0
10
20
30
40
50
60
70

Figure 9

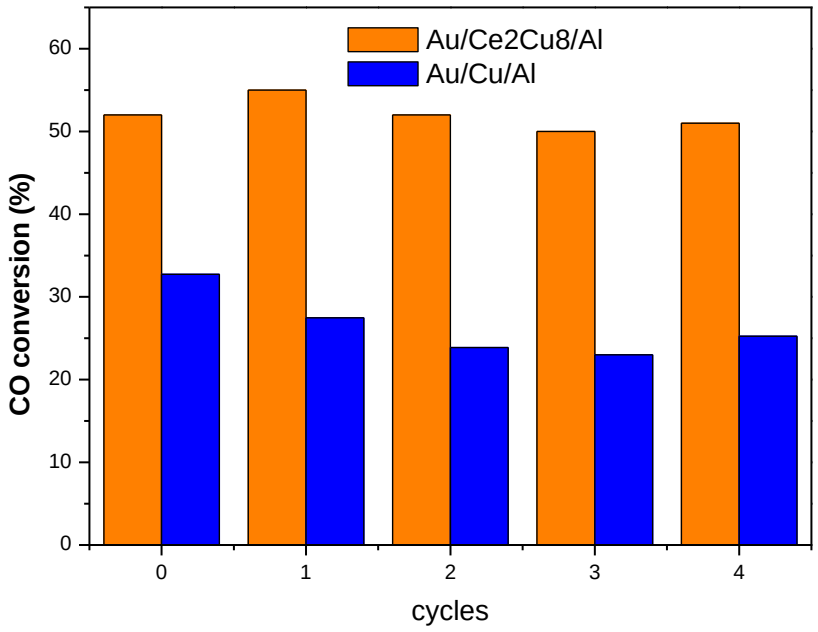
Au/Ce2Cu8/Al
Au/Cu/Al
CO conversion (%)
0
10
20
30
40
50
60
0
1
2
3
4
cycles

Figure 10

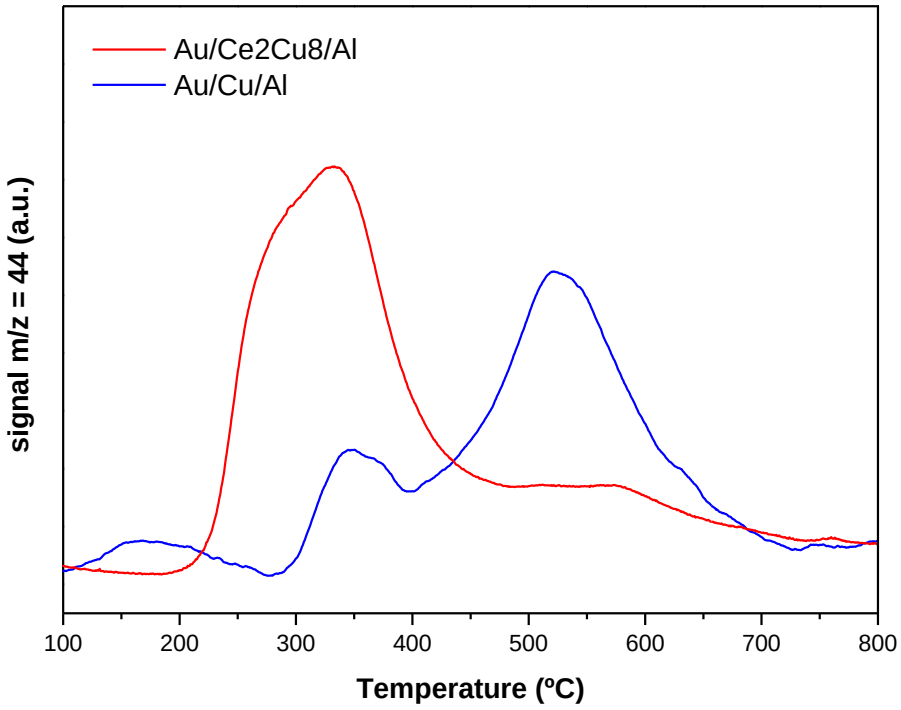
Au/Ce2Cu8/Al
Au/Cu/Al
signal m/z = 44 (a.u.)
100
200
300
400
500
600
700
800
Temperature (ºC)